Science of the Total Environment 740 (2020) 140109

Contents lists available at ScienceDirect

Science of the Total Environment

journal homepage: www.elsevier.com/locate/scitotenv

On the connection between interannual variations of winter haze frequency over Beijing and different ENSO flavors

Jing Wang [a], Yanju Liu [b,*], Yihui Ding [b]

[a] Key Laboratory of Meteorological Disaster, Ministry of Education (KLME), Joint International Research Laboratory of Climate and Environment Change (ILCEC), Collaborative Innovation Center on Forecast and Evaluation of Meteorological Disasters (CIC-FEMD), Nanjing University of Information Science and Technology, Nanjing, China
[b] National Climate Center, China Meteorological Administration, Beijing, China

HIGHLIGHTS

- Haze days in Beijing are more frequent during eastern-Pacific El Niño winters.
- Haze days in Beijing are less frequent during eastern-Pacific La Niña winters.
- Situations of haze days in Beijing are complex in central-Pacific ENSO winters.

GRAPHICAL ABSTRACT

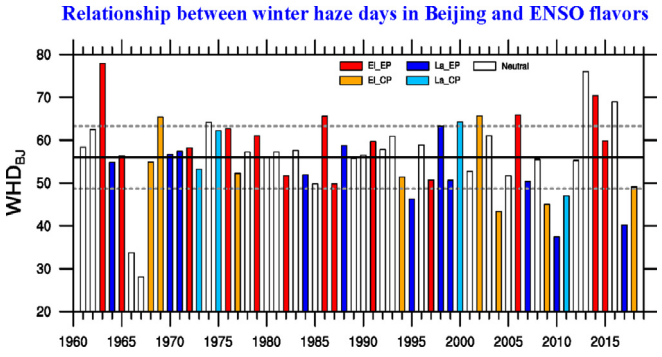

ARTICLE INFO

Article history:
Received 16 March 2020
Received in revised form 8 June 2020
Accepted 8 June 2020
Available online 13 June 2020

Editor: Pingqing Fu

Keywords:
Beijing
Winter haze frequency
Interannual variability
Eastern-Pacific ENSO
Central-Pacific ENSO

ABSTRACT

This study investigated the connection between interannual variations in winter haze frequency over Beijing and different flavors of the El Niño–Southern Oscillation (ENSO). The results showed that the haze frequency was highest during eastern-Pacific (EP) El Niño winters and lowest during EP La Niña winters. No below-normal winter haze frequency years were observed during EP El Niño winters, and no above-normal years were observed during EP La Niña winters. However, the relationship between winter haze frequency and central-Pacific (CP) ENSO conditions was more complex, i.e., both above- and below-normal haze frequency years were equally probable during CP El Niño and CP La Niña winters, and the difference in the number of mean haze days associated with these flavors was exceptionally small. The nearly opposite atmospheric circulation patterns between EP El Niño and EP La Niña winters were responsible for the substantial difference in local winter haze frequency, as these patterns established favorable and unfavorable local meteorological conditions for haze formation, respectively. However, the diverse in situ haze frequency situations during CP El Niño and CP La Niña winters and the small relative differences between such winters could reflect the complexity of the CP ENSO's impacts on haze-related circulation anomalies. The results of this study may help improve winter haze frequency forecasts for Beijing through more accurate climatic predictions.

1. Introduction

Beijing occupies a central political, economic, and cultural role as China's capital. In recent years, however, Beijing and its surroundings have experienced an increasing frequency of haze events (e.g., Ding

* Corresponding author.
E-mail address: liuyanj@cma.gov.cn (Y. Liu).

https://doi.org/10.1016/j.scitotenv.2020.140109
0048-9697/

Table 1
Relationship between the haze frequency over Beijing and ENSO winters with different flavors during 1961–2018.

	El Niño winters (21) [58.6]		La Niña winters (15) [52.3]		Neutral winters (22) [52.4]
	El_EP (13) [63.3]	El_CP (8) [53.9]	La_EP (11) [48.4]	La_CP (4) [56.3]	
Above normal (10)	(4) 1963, 1986, 2006, 2014 **[69.9]**	(2) 1969, 2002 **[65.5]**		(1) 2000 **[64.2]**	(3) 1974, 2013, 2016 **[69.7]**
Normal (40)	(9) 1965, 1972, 1976, 1979, 1982, 1987,1991, 1997, 2015 **[56.7]**	(4) 1968, 1977, 1994, 2018 **[51.9]**	(8) 1964, 1970, 1971, 1984, 1988, 1998, 1999, 2007 **[55.5]**	(2) 1973, 1975 **[57.7]**	(17) 1961, 1962, 1978, 1980, 1981 1983, 1985, 1989, 1990, 1992 1993, 1996, 2001, 2003, 2005, 2008, 2012 **[56.7]**
Below normal (8)		(2) 2004, 2009 **[44.2]**	(3) 1995, 2010, 2017 **[41.3]**	(1) 2011 **[47.0]**	(2) 1966, 1967 **[30.9]**

Notes: Figures within the parentheses indicate the number of years; figures within the brackets are the number or the mean number of winter haze days in Beijing (units in days).

and Liu, 2014; Wang et al., 2018, 2019b). Haze events are often associated with particulate air pollution and low atmospheric visibility (e.g., Ding et al., 2009; An et al., 2019; Wei et al., 2020), and thereby potentially pose harmful effects such as increased deaths from cardiovascular and respiratory diseases (Liu et al., 2019) and increased traffic accidents due to reduced visibility (Chen et al., 2012). Consequently, numerous initiatives—such as the "Ten Statements of Atmosphere" (The State Council of the People's Republic of China, 2013) and the "Three-Year Action Plan for Winning the Blue Sky Defense Battle" (The State Council of the People's Republic of China, 2018)—were promulgated by the Chinese government to mitigate hazy conditions in Beijing.

Climatologically, haze frequency over North China is highest in the boreal winter (e.g., Mao et al., 2019; Chang et al., 2020a). As such, many studies have attempted to identify drivers of winter haze frequency variations over North China to facilitate policymakers in mitigating haze pollution in advance. Previous studies have shown that, aside from anthropogenic influences (e.g., Li et al., 2018b; Zhang et al., 2019), various climatic factors [e.g., monsoon circulations and sea surface temperature (SST)] also play a significant role in modulating localized winter haze frequency over North China (e.g., Li et al., 2016; Wang and Chen, 2016; Cai et al., 2017; Yin et al., 2017; Yin and Wang, 2018; Wang et al., 2020). Particularly noteworthy are several studies on the El Niño–Southern Oscillation (ENSO), a strong oceanic signal modulating interannual wintertime climate variability in East Asian regions (e.g., Wang et al., 2000), including variations in winter haze days (WHDs) in China. The results suggested that El Niño (La Niña) events could result in increased (fewer) WHDs over eastern China (Gao and Li, 2015). Moreover, ensuing studies further suggested that the number of WHDs in southern China is significantly negatively correlated with ENSO, whereas this correlation is insignificant in Beijing and its adjoining areas (Li et al., 2017a; Zhao et al., 2018; He et al., 2019; Cheng et al., 2019). However, more frequent haze days have been reported over North China in late autumn and early winter during certain super El Niño years (e.g., Yuan et al., 2017).

However, the aforementioned studies employed the Niño-3.4 index to delineate evolutions in the ENSO state, and this index poorly differentiates between eastern-Pacific (EP) and central-Pacific (CP) ENSO events (Ren and Jin, 2011). Notably, CP ENSO events have been frequently observed in recent years (Yeh et al., 2009; Wang et al., 2019a), and such events can exert differentiated climatological impacts on eastern China compared with those of traditional EP ENSO events (e.g., Zhang et al., 2014b). Thus, we aimed to reconsider the ENSO's influence on haze variability by considering EP and CP ENSO events separately. Given Beijing's prominence in North China, we focused on elucidating the relationship between the number of WHDs in Beijing (WHD_{BJ}) and different ENSO flavors on the interannual timescale, with the goal of supporting more accurate seasonal forecasts of winter hazy conditions over the Beijing area. Several novel findings were obtained and are presented in the following sections. The rest of this text is structured as follows. Section 2 describes the material and methods. Section 3 describes the connection between winter haze frequency over Beijing and differently flavored ENSO events along with potential associated mechanisms. Conclusions and discussion are given in Section 4.

2. Data and methods

2.1. Data

The datasets used in this study include (1) ground-timing observations at Beijing station (station number: 54511) recorded during 1961–2019 at 02:00, 08:00, 14:00, and 20:00 BLT (Beijing local time) obtained from the National Meteorological Information Center of China (http://data.cma.cn/); (2) monthly planetary boundary layer

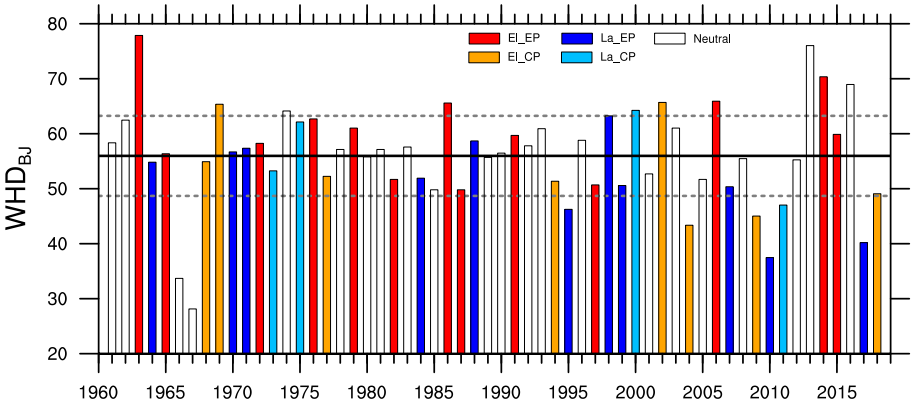

Fig. 1. Time series of the interannual variations of winter haze days in Beijing (WHD_{BJ}) (bars: days) during 1961–2018; different colors indicate different flavors of ENSO winters. The black solid line delineates the average annual WHD_{BJ}, and the gray dashed lines denote 0.8 standard deviation. Here, El_EP (El_CP) and La_EP (La_CP) denote eastern-Pacific (central-Pacific) El Niño winters and eastern-Pacific (central-Pacific) La Niña winters, respectively.

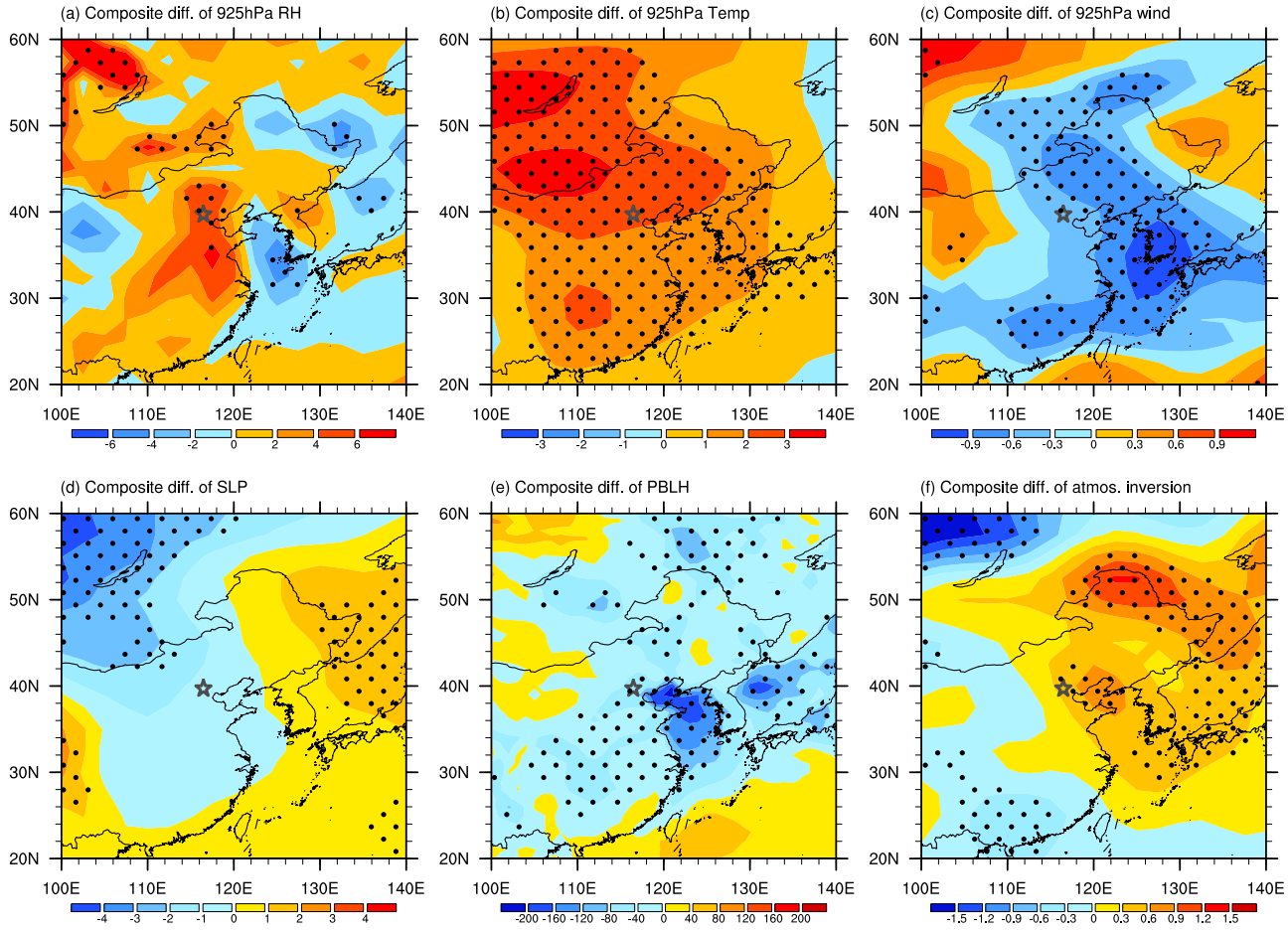

Fig. 2. The December–January–February composite differences in (a) 925-hPa humidity (shading: %), (b) 925-hPa air temperature (shading: °C), (c) 925-hPa wind speed (shading: m s^{-1}), (d) sea-level pressure (shading: hPa), (e) planetary boundary layer height (shading: m) and (f) air temperature between 850 and 1000 hPa (shading: °C) between years with above-normal and below-normal haze frequency. The stippled areas indicate values exceeding the 90% confidence level. The pentagram delineates the location of Beijing.

height (PBLH) for 1979–2019 with a 1° × 1° horizontal resolution from the European Centre for Medium-Range Weather Forecasts Interim Reanalysis (ERA-Interim) (Dee et al., 2011); (3) monthly atmospheric data for 1961–2019 with a 2.5° × 2.5° horizontal resolution from the National Centers for Environmental Prediction (NCEP)–National Center for Atmospheric Research (NCAR) Reanalysis I (NCEP/NCAR) (Kalnay et al., 1996); (4) monthly Hadley Centre SST (HadISST) data for 1961–1981 with a 1° × 1° horizontal resolution (Rayner et al., 2003); and the monthly Optimum Interpolation SST dataset version 2 (OISST v2) for 1982–2019 with a 1° × 1° horizontal resolution from the National Oceanic and Atmospheric Administration (NOAA) (Reynolds et al., 2002).

2.2. Method

Haze days in Beijing were defined as in previous studies (e.g., Chen and Wang, 2015), according to ground-timing observations of relative humidity, visibility, and wind speed. Although the visibility threshold for the haze phenomenon was slightly modified in 2014 (Yin et al., 2017; Pei et al., 2018), the continuity of the data was not affected.

Following the work of Yu et al. (2019), we identified EP/CP ENSO events by employing the national standard of China formulated by Ren et al. (2017). In accordance with this standard, HadISST and OISST v2 data were used to identify EP/CP ENSO episodes during 1961–1981 and 1982–2019, respectively. Moreover, a series of ENSO indices consisting of the Niño-3.4, Niño-3, and Niño-4 indices were utilized to construct the EP/CP ENSO index, which can detect the onset and termination of EP/CP ENSO events. More details on this identification procedure are presented in Ren et al. (2017) and Yu et al. (2019). Here, the boreal winter refers to the seasonal mean for December–January–February (DJF). For instance, the winter of 1961 refers to December 1961 to February 1962. Further, because ENSO episodes usually mature in the boreal winter (Wang et al., 2000), we examined the relationship between the winter haze frequency over Beijing and concurrent ENSO winters with different flavors. Twenty-one El Niño winters, 15 La Niña winters, and 22 neutral winters were classified and are listed in Table 1. Note that El_EP (El_CP) and La_EP (La_CP) denote EP (CP) El Niño winters and EP (CP) La Niña winters, respectively (Table 1).

The interannual component of WHD_{BJ} was extracted by removing the interdecadal constituents of the raw time series of WHD_{BJ}. We used the 9-yr running mean method to obtain the corresponding interdecadal component. Because the first four years and the last four years of the interdecadal component of the WHD_{BJ} are unavailable, an estimation algorithm was employed to resolve the tapering problem caused by the missing years when computing the running mean (Zhu and Li, 2017). For example, the interdecadal component of the WHD_{BJ} for 2017 and 2018 can be obtained based on the mean of 2013–2018 and 2014–2018, respectively. Moreover, to exclude the possible impacts of long-term trends, all data were linearly detrended before analyses. The two-tailed Student's *t*-test was used to evaluate statistical significance.

3. Results

3.1. Associations between WHD_{BJ} and different flavors of ENSO

Fig. 1 illustrates the time series of the interannual variations of WHD_{BJ} during ENSO winters with different flavors (1961–2018). The

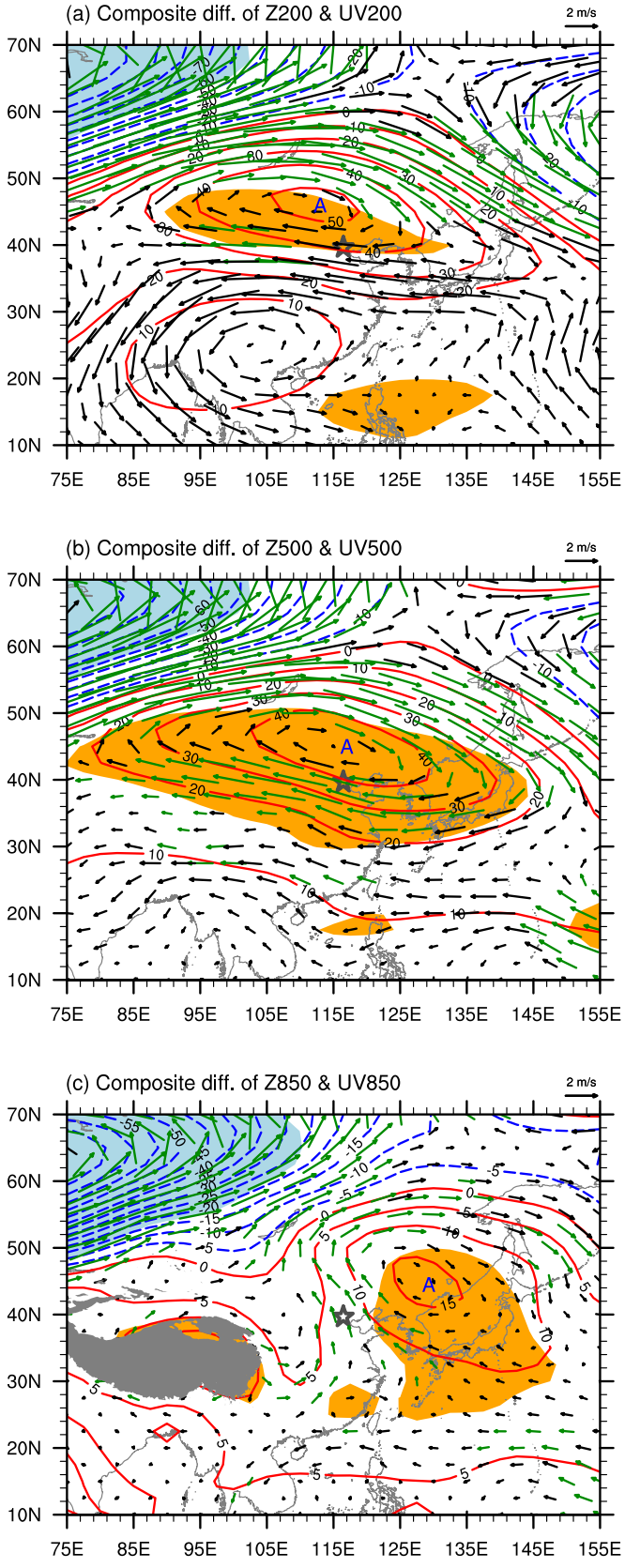

Fig. 3. The December–January-February composite differences of geopotential height (contours: gpm) and winds (vectors: m s $^{-1}$) between years with above-normal and below-normal haze frequency at (a) 200 hPa, (b) 500 hPa, and (c) 850 hPa. Green arrows represent the wind vectors with statistical significance above the 90% confidence level. The orange shaded areas indicate height anomalies exceeding the 95% confidence level. The letter A represents the center of an anticyclonic anomaly. The gray shaded area denotes the Tibetan Plateau, and the pentagram delineates the location of Beijing. (For interpretation of the references to colour in this figure legend, the reader is referred to the web version of this article.)

mean annual number of WHD_{BJ} was 50.0 days, and one corresponding standard deviation was equal to 9.1 days. For the subsequent statistical and composite analyses, we defined years as having an above-normal (AN) or below-normal (BN) winter haze frequency over Beijing based on a standard deviation threshold of ±0.8 (Fig. 1). Thus, 10 years had an AN haze frequency (1963, 1969, 1974, 1986, 2000, 2002, 2006, 2013, 2014, and 2016), 8 years had a BN haze frequency (1966, 1967, 1995, 2004, 2009, 2010, 2011, and 2017), and the other 40 years were deemed normal years (Table 1).

Furthermore, Table 1 shows that the mean numbers of WHD_{BJ} in El Niño, La Niña, and neutral winters were 58.6, 52.3, and 52.4, respectively, indicating relatively little variation. This could partially explain why the correlation between ENSO events and haze frequency over North China has been determined to be insignificant when calculated based on the regular Niño-3.4 index. However, when considering different ENSO flavors, the highest average number of WHD_{BJ} (63.3 days) and the highest number of years with an AN haze frequency [4 out of 10 (40.0%); 69.9 days] were identified during El_EP winters (Table 1), during which no BN in situ haze frequency years were observed (Fig. 1). In stark contrast, the lowest number of mean WHD_{BJ} (48.4 days) and the highest number of years with a BN haze frequency [3 out of 8 (37.5%); 41.3 days] were identified during La_EP winters (Table 1), during which no AN local haze frequency years occurred (Fig. 1). However, the effects of CP ENSO conditions were more complex, and no simple correlations were identified between WHD_{BJ} and El_CP/La_CP. Both AN and BN frequency years were equally probable during El_CP or La_CP winters (Fig. 1); further, only a small difference was found in the mean number of WHD_{BJ} between El_CP and La_CP (Table 1; 53.9 days versus 56.3 days).

Thus, the results suggest the two following questions. First, why are haze frequency conditions over Beijing more diverse in CP ENSO winters than in EP ENSO winters? Second, why is there a significant disparity between the haze frequency during El_EP and La_EP winters but only a slight difference between haze frequency in El_CP and La_CP winters? These questions were addressed by the analyses described below. For convenience, years with an AN (BN) haze frequency within El_EP (La_EP) are referred to as El_EP_H (La_EP_L), while years with an AN (BN) frequency within El_CP are referred to as El_CP_H (EL_CP_L); years with an AN (BN) frequency within La_CP are referred to as La_CP_H (La_CP_L).

3.2. Relevant background on atmospheric anomalies

Because haze variability over eastern China is associated with a variety of climatic factors, including large-scale circulations [e.g., the East Asian winter monsoon (EAWM)] and local-scale dynamic and thermodynamic meteorological parameters (e.g., surface relative humidity and air temperature) (e.g., Wang et al., 2018, 2019b, 2020; Zhang et al., 2014a; Ding et al., 2017; Wu et al., 2017; Zhang, 2017; Chang et al., 2020b), it is appropriate to consider the effects of major atmospheric anomalies before delving into the distinctive impacts of different ENSO flavors on interannual variability in haze frequency over Beijing.

Fig. 2 presents DJF composite differences related to meteorological parameters within the boundary layer. The AN haze frequency is clearly connected to significant near-surface warmer and moister conditions (Fig. 2a, b) as well as stable atmospheric stratification at lower levels (Fig. 2f), in conjunction with negative near-surface wind and PBLH anomalies (Fig. 2c, e). A marked mid-latitude east-west dipole sea-level pressure (SLP) pattern (Fig. 2d) with significant negative (positive) SLP anomalies around the Lake Baikal (Sea of Japan) is also shown. As such, Beijing and its surroundings are controlled by southerly anomalies in the lower troposphere (Fig. 3c), favoring the transportation and accumulation of copious amounts of local and nonlocal aerosols and water vapor over Beijing (Wang et al., 2020). Such environmental conditions could stimulate a striking positive feedback loop effect

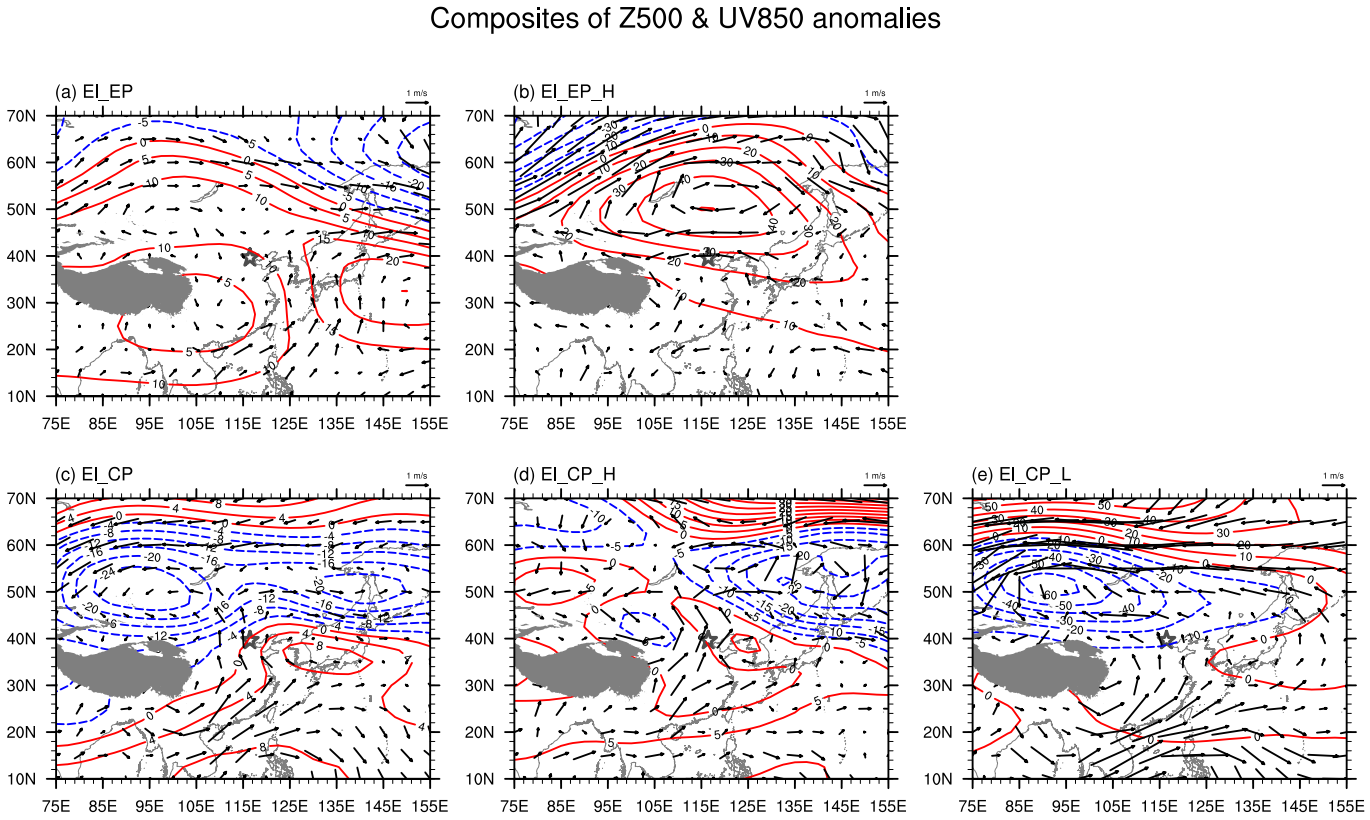

Fig. 4. Composite December–January-February anomalies at a 500-hPa geopotential height (contours: gpm) and 850-hPa winds (vectors: m s^{-1}) for (a) El_EP, (b) El_EP_H, (c) El_CP, (d) El_CP_H, and (e) El_CP_L. Variable anomalies were calculated as the deviation from the 58-yr climatological mean (1961–2018). The gray shaded area denotes the Tibetan Plateau, and the pentagram delineates the location of Beijing.

between localized surface-layer parameters (e.g., temperature, relative humidity, and PBLH) and airborne aerosols, thereby enhancing haze frequency (Li et al., 2017b; An et al., 2019). We found that a significant DJF Northeast Asian anticyclonic anomaly (NEAACA) was the crucial system impacting these anomalous parameters (Fig. 3). The NEAACA is centered to the north of Beijing in the middle and upper troposphere (Figs. 3a, b), while the low-level NEAACA is centered to the northeast of Beijing (Fig. 3c). Essentially, the emergence of the NEAACA denotes a weakened EAWM with a weakened upper-tropospheric westerly jet that shifts more northward (Fig. 3a) (Li et al., 2016; Yin et al., 2017) and suppresses the East Asian major trough (Fig. 3b) (Wang et al., 2020). Thus, the weakened westerly jet suppresses baroclinic instability and is unfavorable for synoptic disturbances (Li et al., 2016), which is in turn conducive to more frequent WHD_{BJ}. Further, a weakened EAWM could favor the establishment of low-level southerly anomalies over Beijing (Fig. 3c). As such, the intrusion of mid-to-high latitude cold and pristine air into Beijing is greatly inhibited. Meanwhile, the resultant amassed aerosols and water vapor that are induced by anomalous southerlies on the western flank of NEAACA can result in a higher number of WHD_{BJ} via the above-mentioned conducive meteorological conditions. Contrasting conditions have been observed in years with BN haze frequency.

3.3. Potential mechanisms of ENSO-related impacts on WHD_{BJ}

Since haze mainly occurs in the lower troposphere, upper tropospheric circulation anomalies were not discussed. Fig. 4 depicts composites of DJF anomalies at a 500-hPa geopotential height and 850-hPa winds during different types of El Niño winters. In general, positive height anomalies predominate throughout Northeast Asia in El_EP, with a notable mid-tropospheric ridge around Lake Baikal (Fig. 4a). In addition, a prominent anticyclonic anomaly centered to the east of Japan and a notable low pressure anomaly centered to the southeast of the Tibetan Plateau can be detected. This strengthening pressure gradient favors the formation of low-level southeasterly winds over Beijing and adjacent regions (Fig. 4a), thus suppressing local cold air activity. As a result, anomalously warm and humid conditions can be experienced around Beijing (Fig. 5, a1, a2). Weak positive wind anomalies were observed around Beijing (Fig. 5, a3), and we found that these wind anomalies were linked to surface northerly wind anomalies in terms of a clear corresponding positive zonal SLP anomaly (Fig. 5, a4). However, these northerlies (not shown) are quite shallow. Therefore, they cannot effectively decrease the near-surface temperature (Fig. 5, a2) but are indicative of downward motion over Beijing and its surroundings (Wu et al., 2017). Under such conditions, positive stable atmospheric stratification at lower levels and below-average PBLH over Beijing can be induced (Fig. 5, a5, a6). Overall, these environmental conditions are fairly conducive to more frequent WHD_{BJ}. Furthermore, the composite mid-tropospheric NEAACA, which is quite similar to its counterpart shown in Fig. 3b, can be discerned in some EP El Niño winters (Fig. 4b). Although anomalous southerlies are not established (Fig. 4b) as shown in Fig. 3c, notably strong easterlies carrying abundant warmer moisture from the ocean and marginal seas can be established, dampening both the climatological westerly wind component of the EAWM and the low-level wind speed around Beijing and thereby favoring the in situ agglomeration of pollutants (Lou et al., 2019). As such, considerably more favorable environmental circumstances for in situ haze occurrence can be induced (Fig. 5, c1–c6). This NEAACA (Fig. 4b) exhibits a stronger barotropic structure compared with that in Fig. 3 due to the distribution of low-level winds. Numerous studies have demonstrated the existence of an anomalous anticyclone in association with El Niño (e.g., Zhang et al., 1996; Wang and Zhang, 2002); however, no anomalous anticyclone is shown in the lower troposphere over the western North Pacific (WNP) in Fig. 4b as it is in Fig. 4a. The reason may be

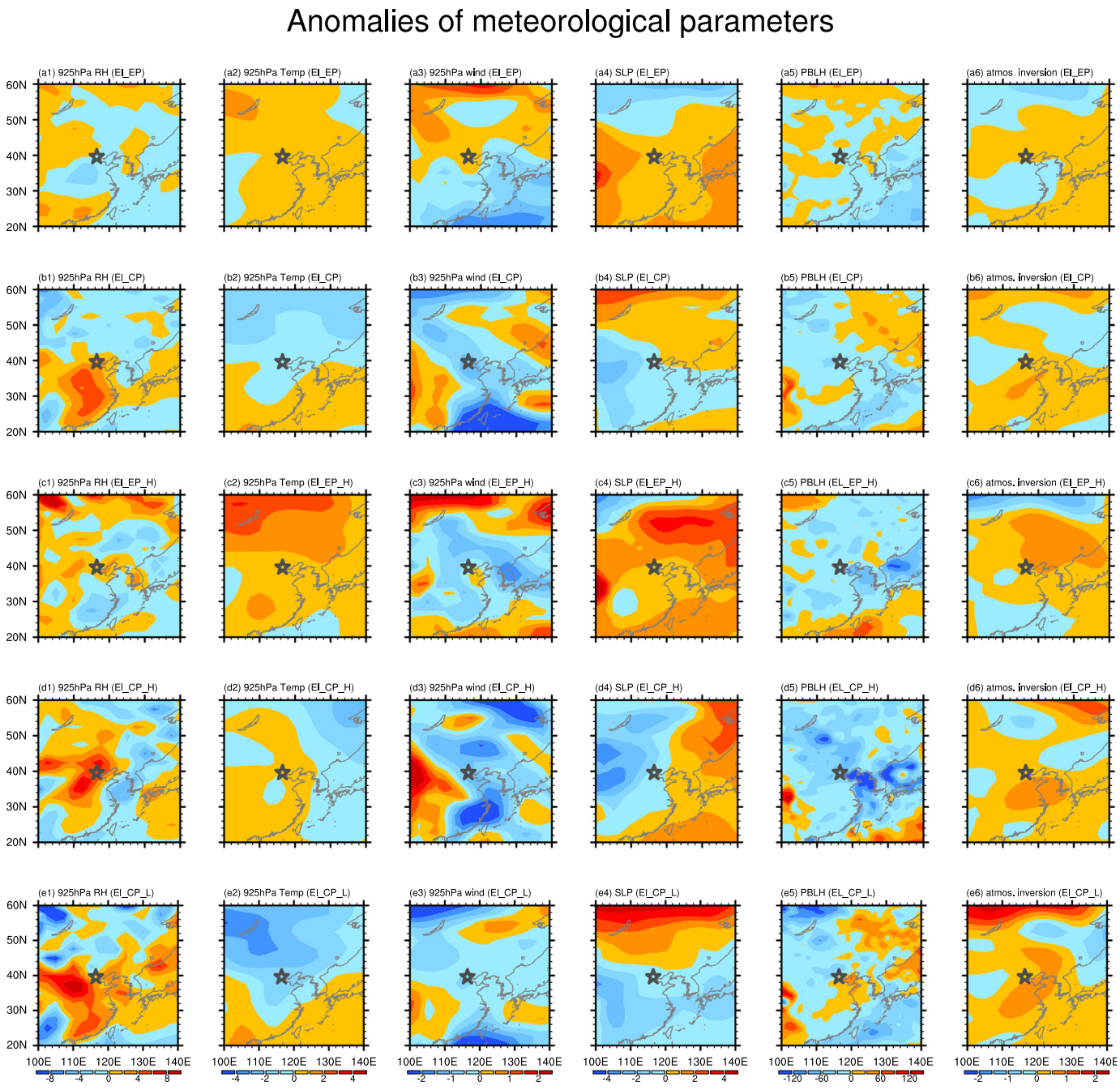

Fig. 5. Composite December–January-February anomalies in 925-hPa relative humidity (%), 925-hPa air temperature (°C), 925-hPa wind speed (m s^{-1}), sea-level pressure (hPa), planetary boundary layer height (m) and air temperature between 850 and 1000 hPa (°C) for (a1–a6) El_EP, (b1–b6) El_CP, (c1–c6) El_EP_H, (d1–d6) El_CP_H, and (e1–e6) El_CP_L. Anomalies for variables were calculated as the deviation from the 58-yr climatological mean (1961–2018). The pentagram delineates the location of Beijing.

that the WNP anticyclonic anomaly (WNPACA) is extremely strengthened in Fig. 4b and thus shifts much more northwestward, forming the remarkable NEAACA in conjunction with the anomalous mid-latitude ridge.

However, situations are more complex in El_CP. Unlike in El_EP winters, the broad Northeast Asian region is predominated by significant negative height anomalies (Fig. 4c). Further, positive height anomalies can be found to the east and south of Beijing, with a noticeable composite NEAACA centered over the southern Sea of Japan (Fig. 4c). Concomitant anomalous low-level southerlies prevail from southeastern China to the areas around Beijing can also be discerned. The corresponding meteorological variables, except for decreased near-surface temperature, are conducive to haze formation (Fig. 5, b1–b6). In general, these anomalous southerlies could be associated with positive near-surface temperature anomalies around Beijing. However, the observed negative height anomalies to the north of Beijing (Fig. 4c) suggest the existence of mid-tropospheric stronger cold air activities over mid-to-high latitude areas, which can still decrease the temperature over Beijing (Fig. 5, b2) through the enhanced transportation of cold advection despite the fact that these anomalous southerlies can offset the influence of cold air to some extent. By contrast, in some CP El Niño winters (Fig. 4d), the above NEAACA shifts more westward and is centered around the Shandong Peninsula, leading to more intense southerly anomalies over Beijing. Accordingly, the meteorological variables become far more conducive to haze formation than those in El_CP

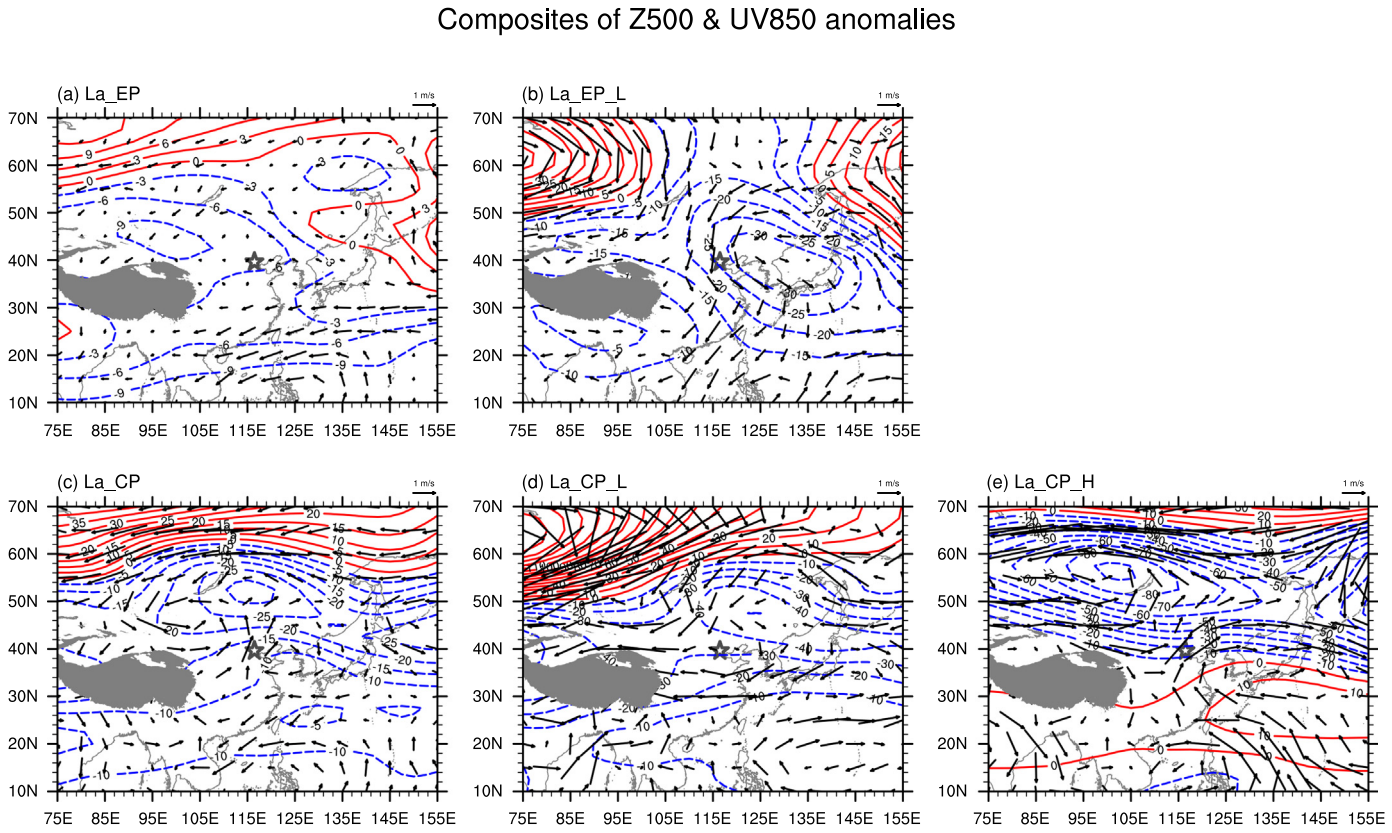

Fig. 6. Composite December–January-February anomalies at a 500-hPa geopotential height (contours: gpm) and 850-hPa winds (vectors: m s^{-1}) for (a) La_EP, (b) La_EP_L, (c) La_CP, (d) La_CP_L, and (e) La_CP_H. Variable anomalies were calculated as the deviation from the 58-yr climatological mean (1961–2018). The gray shaded area denotes the Tibetan Plateau, and the pentagram delineates the location of Beijing.

(Fig. 5, d1–d6), including strengthened positive temperature anomalies (Fig. 5, d2); whereas in other El_CP winters (Fig. 4e), low-level southerly winds are suppressed due to the effects of a dampened NEAACA and enhanced cold air activity, resulting in more unfavorable meteorological conditions for haze formation (Fig. 5, e1–e6), such as notably decreased temperature (Fig. 5, e2) and relative humidity (Fig. 5, e1).

Next, we discuss the distinctive impacts of two types of La Niña winters. In general, circulation patterns between La_EP and El_EP are dramatically reversed in sign (Figs. 6a, 4a), especially between La_EP_L and El_EP_H (Figs. 6b, 4b); these differing circulation patterns could exert widely varied impacts on haze frequency. Due to these antithetical patterns, the parameters associated with La_EP are extremely unfavorable for haze formation (Fig. 7, a1–a6). The composite barotropic Northeast Asian cyclonic anomaly (NEACA) can be discerned in some La_EP winters, triggering extremely strengthened EAWM intensity with significant northerlies (Fig. 6b). This results in extremely unfavorable in situ conditions for haze formation (Fig. 7, c1–c6), and in conjunction with the NEACA, are largely responsible for the above atmospheric anomalies tied to La_EP (Figs. 6a and 7, a1–a6).

Furthermore, the circulation anomalies in La_CP resemble those in El_CP except for the negative height anomalies to the east and south of Beijing (Figs. 6c–e), suggesting colder local conditions. However, a clear low-level NEAACA is centered near the Shandong Peninsula, as implied by the 850-hPa wind anomalies (Fig. 6c), thereby inducing significant southerlies over Beijing to offset the local cold conditions. Consequently, the associated meteorological variables, such as the increased relative humidity and decreased winds, are relatively conducive to haze formation (Fig. 7, b1–b6) compared with those in La_EP (Fig. 7, a1–a6). Similarly, we also discerned diverse patterns associated with La_CP. For example, in the winter of 2000, the aforementioned negative height anomalies were replaced by positive anomalies (Fig. 6e), suggesting an enhanced WNPACA. This WNPACA could have stimulated enhanced southerlies over Beijing and its surrounding area as well as the northward shift of cold air. Thus, the conditions were far more conducive to a higher number of WHD_{BJ} (Fig. 7, e1–e6). However, in the winter of 2011 (Fig. 6d), the enhanced intrusion of a cold air mass dramatically weakened the southerlies and the WNPACA, resulting in highly unfavorable hazy conditions (Fig. 7, d1–d6).

In summary, the atmospheric conditions tied to El_CP/La_CP are variable and inconsistent. Therefore, varied haze frequencies could arise during CP ENSO winters due to CP ENSO's more complicated impacts on haze-related atmospheric anomalies. Additionally, it is significant that the warmest surface temperature anomalies occurred in El_EP. It has been reported that high temperatures favor the formation of secondary aerosols (Jacob and Winner, 2009), which could increase haze frequency. Thus, based on the preceding analyses, we can conclude that the environmental circumstances are most favorable (unfavorable) for haze formation during El_EP (La_EP), which can explain why the highest (lowest) average number of WHD_{BJ} occur during El_EP (La_EP). Further, because of the distinctive influence pathways associated with CP ENSO, both AN and BN frequency years were determined to be equally probable during El_CP and La_CP, resulting in only a minor difference in the mean number of WHD_{BJ} between them.

4. Conclusions and discussion

In this paper, the interannual variability of haze frequency over Beijing and its relationship with different ENSO flavors during the boreal winters of 1961–2018 were investigated. We found that no BN (AN) haze frequency years occurred during El_EP (La_EP), and the corresponding mean number of WHD_{BJ} was highest (lowest) during these winters. However, the impact of CP ENSO winters on WHD_{BJ} was more complex. AN and BN haze frequency years were equally probable

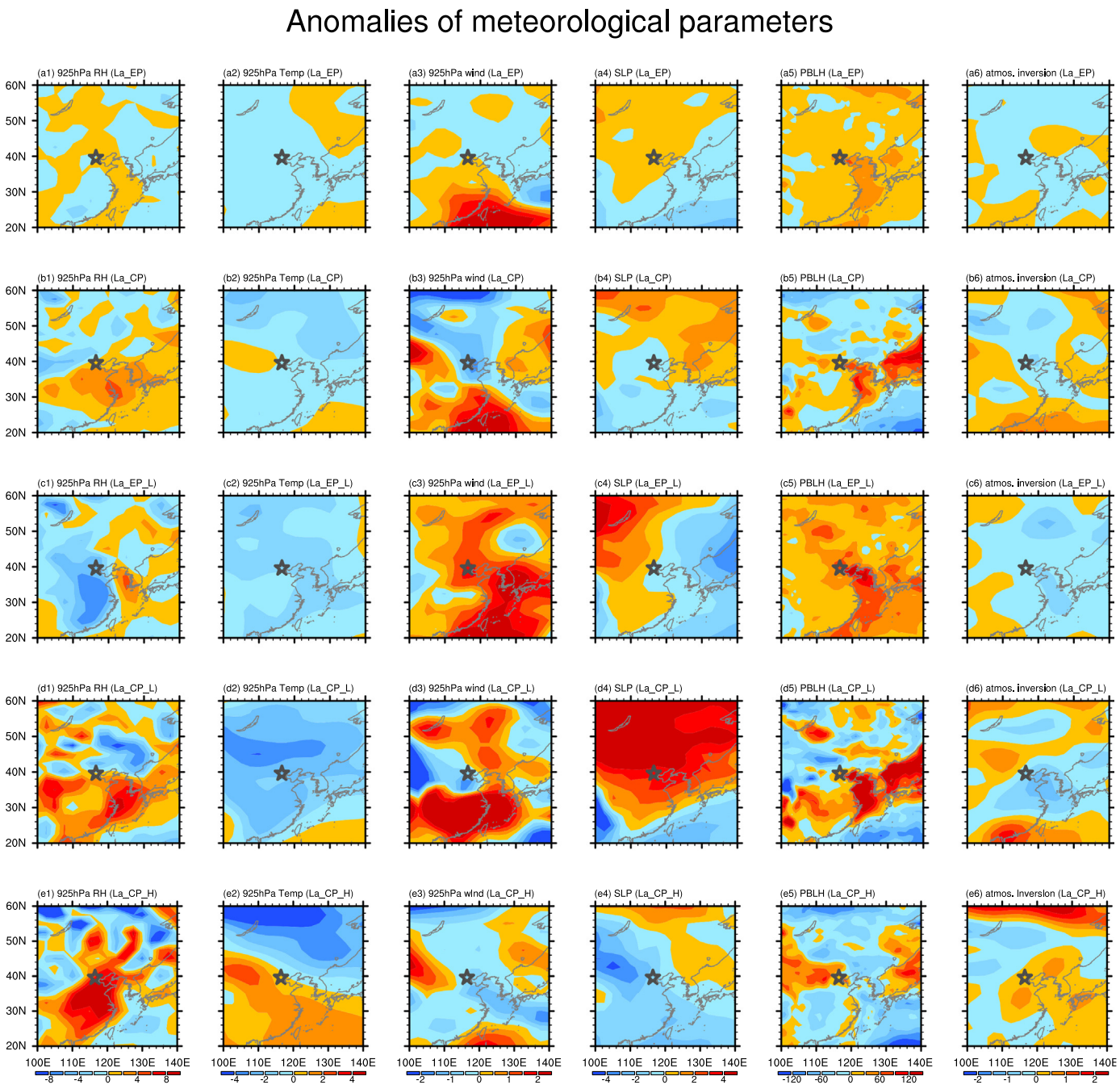

Fig. 7. Composite December–January-February anomalies in 925-hPa relative humidity (%), 925-hPa air temperature (°C), 925-hPa wind speed (m s^{-1}), sea-level pressure (hPa), planetary boundary layer height (m) and air temperature between 850 and 1000 hPa (°C) for (a1–a6) La_EP, (b1–b6) La_CP, (c1–c6) La_EP_L, (d1–d6) La_CP_L, and (e1–e6) La_CP_H. Anomalies for variables were calculated as the deviation from the 58-yr climatological mean (1961–2018). The pentagram delineates the location of Beijing.

during El_CP or La_CP, and the difference in the average number of WHD_{BJ} between these winters was quite small.

Almost completely opposite circulation patterns are observed in El_EP and La_EP winters, and the appearance of NEAACA and NEACA in El_EP_H and La_EP_L, respectively, largely contributes to these opposing patterns. Under such circumstances, the corresponding anomalies of meteorological parameters within the boundary layer were nearly opposite in sign, leading to a considerable difference in the number of WHD_{BJ}. However, more diverse circulation patterns and more distinctive meteorological conditions were detected in El_CP/La_CP, resulting in a more complex connection between WHD_{BJ} and CP El Niño/La Niña winters.

Furthermore, although significant low-level southerly anomalies can offset the effect of cold air activity over Beijing in El_CP and La_CP, the surface temperatures in both El_CP and La_CP are quite lower than those in El_EP. Therefore, the mean number of WHD_{BJ} tends to be highest during El_EP, presumably due to in situ environmental conditions conducive to the formation of haze that are largely induced by the barotropic NEAACA in El_EP_H. Again, lower-than-normal temperature in conjunction with other extremely unfavorable variables (e.g., decreased relative humidity and increased winds and PBLH) during La_EP are responsible for the lowest mean number of WHD_{BJ} during such winters, which is largely tied to the barotropic NEACA in La_EP_L. In addition, both AN and BN frequency years can be seen during El_CP and La_CP, which

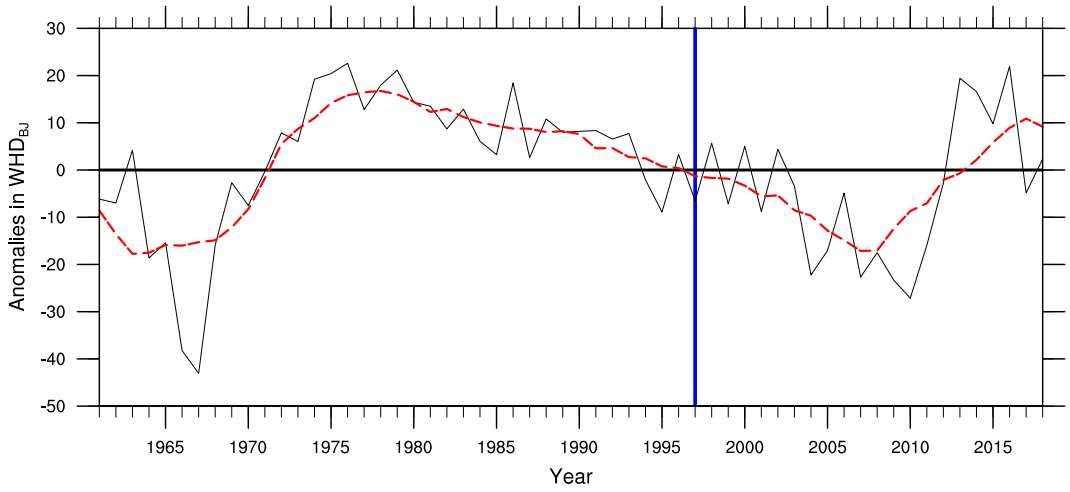

Fig. 8. Time series of anomalies in detrended raw winter haze days in Beijing (black line: days) along with its interdecadal component (red line: days) for 1961–2018. The blue vertical line delineates the year 1997. (For interpretation of the references to colour in this figure legend, the reader is referred to the web version of this article.)

could substantially lower the overall difference in the haze frequency between them. Importantly, the circulation patterns north of about 40°N are fairly consistent between El_CP and La_CP (Figs. 4c, 6c); these patterns differ more strongly between El_EP and La_EP. The differences between El_CP and La_CP are mainly confined to the tropical-extratropical western Pacific, with a conspicuous anticyclonic (cyclonic) anomaly located around the Philippines (Figs. 4c, 6c); this concurs with the results of Li et al. (2018a). However, the similar patterns north of 40°N can contribute to comparable in situ environmental conditions, such as increased relative humidity and decreased temperature (Fig. 5, b1–b2 and Fig. 7, b1–b2), which might also be responsible for the minor differences in haze frequency between El_CP and La_CP.

The clearer physical processes by which ENSO affects WHD$_{BJ}$ can be described as follows. In boreal winters, the EP El Niño (La Niña) is accompanied by an anomalous anticyclone (cyclone) over the WNP, resulting in anomalous southerly (northerly) winds around the southeastern coast of East Asia (Zhang et al., 1996, 2015). The anomalous southerly (northerly) winds weaken (strengthen) the EAWM, and a weak (strong) EAWM corresponds to more (fewer) haze days over eastern China (Li et al., 2016). However, we also identified no consistent effect of CP El Niño winters on the EAWM (Zhang et al., 2017). Therefore, the complex connection between WHD$_{BJ}$ and CP El Niño/La Niña winters in this study was put forward.

However, significant uncertainties may emerge if CP El Niño, especially CP La Niña episodes, are used to conduct seasonal WHD$_{BJ}$ forecasts. This might be because fewer and more diverse events could reduce the robustness of the statistical results, due to the presence of extraneous fluctuations in meteorological conditions. The composite PBLH and atmospheric stability anomalies in La_CP seem more unfavorable for haze formation compared to those in El_CP (Fig. 5, b5–b6 and Fig. 7, b5–b6), but haze frequency in La_CP is somewhat higher. Whether such an unusual phenomenon can be attributed to the abovementioned poor robustness deserves further exploration. As more frequent CP ENSO events are predicted to occur in the future (Wang et al., 2019a), more robust results may be possible in the future.

Finally, a clear decreasing (increasing) trend in the number of EP El Niños (EP La Niñas) was observed since the late 1990s (since around 1997) (Table 1), which concurred with previous studies (Wang et al., 2019a; Zhao and Wang, 2019). Such decadal variabilities could in part explain the significant epochal enhancement (decline) in the number of WHD$_{BJ}$ for 1981–1997 (1998–2014) (Fig. 8). However, a clear decadal decrease and increase were also observed in the frequency of haze events before the early 1970s and after the mid–2010s, respectively. Whether such decadal variations are modulated by other climate factors are intriguing issues that deserve further exploration.

Credit authorship contribution statement

Jing Wang: Methodology, Software, Writing-original draft, Visualization, Investigation. Yanju Liu: Validation, Data curation, Project administration, Funding acquisition, Writing-Reviewing and Editing. Yihui Ding: Conceptualization, Supervision.

Declaration of competing interest

The authors declare that they have no known competing financial interests or personal relationships that could have appeared to influence the work reported in this paper.

Acknowledgments

This work was supported by the Atmospheric Pollution Control of the Prime Minister Fund (Grant No. DQGG0104), the National Natural Science Foundation of China (Grant No. 41790471), the National Basic Research Program of China (973 Program) (Grant No. 2012CB417205), and the Strategic Priority Research Program of Chinese Academy of Sciences (Grant No. XDA20100304).

References

An, Z., Huang, R.-J., Zhang, R., Tie, X., Li, G., Cao, J., Zhou, W., Shi, Z., Han, Y., Gu, Z., Ji, Y., 2019. Severe haze in northern China: a synergy of anthropogenic emissions and atmospheric processes. Proc. Natl. Acad. Sci. U. S. A. 116 (18), 8657–8666.

Cai, W.J., Li, K., Liao, H., Wang, H.J., Wu, L.X., 2017. Weather conditions conducive to Beijing severe haze more frequent under climate change. Nat. Clim. Chang. 7 (4), 257–262.

Chang, L., Wu, Z., Xu, J., 2020a. A comparison of haze pollution variability in China using haze indices based on observations. Sci. Total Environ. 715, 136929.

Chang, Y., Wang, J., Zhu, Z., Deng, H., He, J., Lu, R., 2020b. A salient oceanic driver for the interannual variability of wintertime haze days over the Pearl River Delta region, China. Theor. Appl. Climatol. 140 (1), 739–750.

Chen, H.P., Wang, H.J., 2015. Haze days in North China and the associated atmospheric circulations based on daily visibility data from 1960 to 2012. J. Geophys. Res.-Atmos. 120 (12), 5895–5909.

Chen, J., Zhao, C.S., Ma, N., Liu, P.F., Göbel, T., Hallbauer, E., Deng, Z.Z., Ran, L., Xu, W.Y., Liang, Z., Liu, H.J., Yan, P., Zhou, X.J., Wiedensohler, A., 2012. A parameterization of low visibilities for hazy days in the North China Plain. Atmos. Chem. Phys. 12 (11), 4935–4950.

Cheng, X., Boiyo, R., Zhao, T., Xu, X., Gong, S., Xie, X., Shang, K., 2019. Climate modulation of Niño3.4 SST-anomalies on air quality change in southern China: application to seasonal forecast of haze pollution. Atmos. Res. 225, 157–164.

Dee, D.P., Uppala, S.M., Simmons, A.J., Berrisford, P., Poli, P., Kobayashi, S., Andrae, U., Balmaseda, M.A., Balsamo, G., Bauer, P., Bechtold, P., Beljaars, A.C.M., van de Berg, L., Bidlot, J., Bormann, N., Delsol, C., Dragani, R., Fuentes, M., Geer, A.J., Haimberger, L., Healy, S.B., Hersbach, H., Hólm, E.V., Isaksen, L., Kållberg, P., Köhler, M., Matricardi, M., McNally, A.P., Monge-Sanz, B.M., Morcrette, J.J., Park, B.K., Peubey, C., de Rosnay,

P., Tavolato, C., Thépaut, J.N., Vitart, F., 2011. The ERA-interim reanalysis: configuration and performance of the data assimilation system. Q. J. R. Meteorol. Soc. 137, 553–597.
Ding, Y.H., Liu, Y.J., 2014. Analysis of long-term variations of fog and haze in China in recent 50 years and their relations with atmospheric humidity. Sci. China Earth Sci. 57 (1), 36–46.
Ding, Y.H., Li, Q.P., Liu, Y.J., Zhang, L., Song, Y.F., Zhang, J., 2009. Atmospheric aerosols, air pollution and climate change (in Chinese). Meteorological Monthly 35 (3), 3–15.
Ding, Y.H., Wu, P., Liu, Y.J., Song, Y.F., 2017. Environmental and dynamic conditions for the occurrence of persistent haze events in North China. Engineering 3 (2), 266–271.
Gao, H., Li, X., 2015. Influences of El Nino southern oscillation events on haze frequency in eastern China during boreal winters. Int. J. Climatol. 35 (9), 2682–2688.
He, C., Liu, R., Wang, X.M., Liu, S.C., Zhou, T.J., Liao, W.H., 2019. How does El Niño-southern oscillation modulate the interannual variability of winter haze days over eastern China? Sci. Total Environ. 651, 1892–1902.
Jacob, D.J., Winner, D.A., 2009. Effect of climate change on air quality. Atmos. Environ. 43 (1), 51–63.
Kalnay, E., Kanamitsu, M., Kistler, R., Collins, W., Deaven, D., Gandin, L., Iredell, M., Saha, S., White, G., Woollen, J., Zhu, Y., Chelliah, M., Ebisuzaki, W., Higgins, W., Janowiak, J., Mo, K.C., Ropelewski, C., Wang, J., Leetmaa, A., Reynolds, R., Jenne, R., Joseph, D., 1996. The NCEP/NCAR 40-year reanalysis project. Bull. Am. Meteorol. Soc. 77 (3), 437–471.
Li, Q., Zhang, R.H., Wang, Y., 2016. Interannual variation of the wintertime fog–haze days across central and eastern China and its relation with East Asian winter monsoon. Int. J. Climatol. 36 (1), 346–354.
Li, S.L., Han, Z., Chen, H.P., 2017a. A comparison of the effects of interannual Arctic sea ice loss and ENSO on winter haze days: observational analyses and AGCM simulations. Journal of Meteorological Research 31 (5), 820–833.
Li, Z., Guo, J., Ding, A., Liao, H., Liu, J., Sun, Y., Wang, T., Xue, H., Zhang, H., Zhu, B., 2017b. Aerosol and boundary-layer interactions and impact on air quality. Natl. Sci. Rev. 4 (6), 810–833.
Li, J., Huang, D., Li, F., Wen, Z., 2018a. Circulation characteristics of EP and CP ENSO and their impacts on precipitation in south China. J. Atmos. Sol. Terr. Phys. 179, 405–415.
Li, K., Liao, H., Cai, W.J., Yang, Y., 2018b. Attribution of anthropogenic influence on atmospheric patterns conducive to recent most severe haze over eastern China. Geophys. Res. Lett. 45 (4), 2072–2081.
Liu, C., Chen, R., Sera, F., Vicedo-Cabrera, A.M., Guo, Y., Tong, S., Coelho, M.S.Z.S., Saldiva, P.H.N., Lavigne, E., Matus, P., Valdes Ortega, N., Osorio Garcia, S., Pascal, M., Stafoggia, M., Scortichini, M., Hashizume, M., Honda, Y., Hurtado-Díaz, M., Cruz, J., Nunes, B., Teixeira, J.P., Kim, H., Tobias, A., Íñiguez, C., Forsberg, B., Åström, C., Ragettli, M.S., Guo, Y.-L., Chen, B.-Y., Bell, M.L., Wright, C.Y., Scovronick, N., Garland, R.M., Milojevic, A., Kyselý, J., Urban, A., Orru, H., Indermitte, E., Jaakkola, J.J.K., Ryti, N.R.I., Katsouyanni, K., Analitis, A., Zanobetti, A., Schwartz, J., Chen, J., Wu, T., Cohen, A., Gasparrini, A., Kan, H., 2019. Ambient particulate air pollution and daily mortality in 652 cities. N. Engl. J. Med. 381 (8), 705–715.
Lou, S., Yang, Y., Wang, H., Smith, S.J., Qian, Y., Rasch, P.J., 2019. Black carbon amplifies haze over the North China Plain by weakening the East Asian winter monsoon. Geophys. Res. Lett. 46 (1), 452–460.
Mao, L., Liu, R., Liao, W., Wang, X., Shao, M., Liu, S.C., Zhang, Y., 2019. An observation-based perspective of winter haze days in four major polluted regions of China. Natl. Sci. Rev. 6 (3), 515–523.
Pei, L., Yan, Z.W., Sun, Z.B., Miao, S.G., Yao, Y., 2018. Increasing persistent haze in Beijing: potential impacts of weakening East Asian winter monsoons associated with northwestern Pacific sea surface temperature trends. Atmos. Chem. Phys. 18 (5), 3173–3183.
Rayner, N.A., Parker, D.E., Horton, E.B., Folland, C.K., Alexander, L.V., Rowell, D.P., Kent, E.C., Kaplan, A., 2003. Global analyses of sea surface temperature, sea ice, and night marine air temperature since the late nineteenth century. J. Geophys. Res. 108 (D14), 4407.
Ren, H.-L., Jin, F.-F., 2011. Niño indices for two types of ENSO. Geophys. Res. Lett. 38 (4), L04704.
Ren, H., Sun, C., Ren, F., et al., 2017. Identification method for El Niño/La Niña events. The People's Republic China's National Standard GB/T 33666–2017, May 2017. Standards Press of China, Beijing, pp. 1–6.
Reynolds, R.W., Rayner, N.A., Smith, T.M., Stokes, D.C., Wang, W., 2002. An improved in situ and satellite SST analysis for climate. J. Clim. 15 (13), 1609–1625.
The State Council of the People's Republic of China, 2013. Air pollution prevention and control action plan. Chinese. http://www.gov.cn/zwgk/2013-09/12/content_2486773.htm.
The State Council of the People's Republic of China, 2018. Notice of the state council on issuing the three-year action plan for winning the blue sky defense battle. in Chinese. http://www.gov.cn/zhengce/content/2018-07/03/content_5303158.htm.
Wang, H.J., Chen, H.P., 2016. Understanding the recent trend of haze pollution in eastern China: roles of climate change. Atmos. Chem. Phys. 16 (6), 4205–4211.
Wang, B., Zhang, Q., 2002. Pacific–East Asian teleconnection. Part II: how the Philippine Sea anomalous anticyclone is established during El Niño development. J. Clim. 15 (22), 3252–3265.
Wang, B., Wu, R.G., Fu, X.H., 2000. Pacific–East Asian teleconnection: how does ENSO affect East Asian climate? J. Clim. 13 (9), 1517–1536.
Wang, J., Zhao, Q.H., Zhu, Z.W., Qi, L., Wang, J.X.L., He, J.H., 2018. Interannual variation in the number and severity of autumnal haze days in the Beijing–Tianjin–Hebei region and associated atmospheric circulation anomalies. Dyn. Atmos. Oceans 84, 1–9.
Wang, B., Luo, X., Yang, Y.-M., Sun, W., Cane, M.A., Cai, W., Yeh, S.-W., Liu, J., 2019a. Historical change of El Niño properties sheds light on future changes of extreme El Niño. Proc. Natl. Acad. Sci. U. S. A. 116 (45), 22512–22517.
Wang, J., Zhu, Z.W., Qi, L., Zhao, Q.H., He, J.H., Wang, J.X.L., 2019b. Two pathways of how remote SST anomalies drive the interannual variability of autumnal haze days in the Beijing–Tianjin–Hebei region, China. Atmos. Chem. Phys. 19 (3), 1521–1535.
Wang, J., Liu, Y., Ding, Y., Wu, P., Zhu, Z., Xu, Y., Li, Q., Zhang, Y., He, J., Wang, J.X.L., Qi, L., 2020. Impacts of climate anomalies on the interannual and interdecadal variability of autumn and winter haze in North China: a review. Int. J. Climatol. https://doi.org/10.1002/joc.6471.
Wei, K., Tang, X., Tang, G., Wang, J., Xu, L., Li, J., Ni, C., Zhou, Y., Ding, Y., Liu, W., 2020. Distinction of two kinds of haze. Atmos. Environ. 223, 117228.
Wu, P., Ding, Y.H., Liu, Y.J., 2017. Atmospheric circulation and dynamic mechanism for persistent haze events in the Beijing-Tianjin-Hebei region. Adv. Atmos. Sci. 34 (4), 429–440.
Yeh, S.-W., Kug, J.-S., Dewitte, B., Kwon, M.-H., Kirtman, B.P., Jin, F.-F., 2009. El Niño in a changing climate. Nature 461 (7263), 511–514.
Yin, Z., Wang, H., 2018. The strengthening relationship between Eurasian snow cover and December haze days in central North China after the mid-1990s. Atmos. Chem. Phys. 18 (7), 4753–4763.
Yin, Z., Wang, H., Chen, H., 2017. Understanding severe winter haze events in the North China plain in 2014: roles of climate anomalies. Atmos. Chem. Phys. 17 (3), 1641–1651.
Yu, X.C., Wang, Z.L., Zhang, H., Zhao, S.Y., 2019. Impacts of different types and intensities of El Niño events on winter aerosols over China. Sci. Total Environ. 655, 766–780.
Yuan, Y., Zhou, N.F., Li, C.Y., 2017. Correlation between haze in North China and super El Niño events (in Chinese). Chin. J. Geophys. 60 (1), 11–21.
Zhang, R., 2017. Warming boosts air pollution. Nat. Clim. Chang. 7, 238–239.
Zhang, R., Sumi, A., Kimoto, M., 1996. Impact of El Niño on the east Asian monsoon: a diagnostic study of the '86/87 and '91/92 events. J. Meteorol. Soc. Jpn. 74 (1), 49–62.
Zhang, R.H., Li, Q., Zhang, R.N., 2014a. Meteorological conditions for the persistent severe fog and haze event over eastern China in January 2013. Sci. China Earth Sci. 57 (1), 26–35.
Zhang, W., Jin, F.-F., Turner, A., 2014b. Increasing autumn drought over southern China associated with ENSO regime shift. Geophys. Res. Lett. 41 (11), 4020–4026.
Zhang, R., Li, T., Wen, M., Liu, L., 2015. Role of intraseasonal oscillation in asymmetric impacts of El Niño and La Niña on the rainfall over southern China in boreal winter. Clim. Dyn. 45 (3), 559–567.
Zhang, R., Min, Q., Su, J., 2017. Impact of El Niño on atmospheric circulations over East Asia and rainfall in China: role of the anomalous western North Pacific anticyclone. Sci. China Earth Sci. 60 (6), 1124–1132.
Zhang, Q., Zheng, Y., Tong, D., Shao, M., Wang, S., Zhang, Y., Xu, X., Wang, J., He, H., Liu, W., Ding, Y., Lei, Y., Li, J., Wang, Z., Zhang, X., Wang, Y., Cheng, J., Liu, Y., Shi, Q., Yan, L., Geng, G., Hong, C., Li, M., Liu, F., Zheng, B., Cao, J., Ding, A., Gao, J., Fu, Q., Huo, J., Liu, B., Liu, Z., Yang, F., He, K., Hao, J., 2019. Drivers of improved $PM_{2.5}$ air quality in China from 2013 to 2017. Proc. Natl. Acad. Sci. U. S. A. 116 (49), 24463–24469.
Zhao, H., Wang, C., 2019. On the relationship between ENSO and tropical cyclones in the western North Pacific during the boreal summer. Clim. Dyn. 52 (1), 275–288.
Zhao, S.Y., Zhang, H., Xie, B., 2018. The effects of El Niño–southern oscillation on the winter haze pollution of China. Atmos. Chem. Phys. 18 (3), 1863–1877.
Zhu, Z.W., Li, T., 2017. The record-breaking hot summer in 2015 over Hawaii and its physical causes. J. Clim. 30 (11), 4253–4266.